University of Groningen

Electromagnetic response functions in proton-proton scattering

Kiš, Mladen

Publication date:
2005

Chapter 2

Virtual bremsstrahlung reaction

In this chapter we introduce the theoretical models that describe the virtual bremsstrahlung process. The observables used to describe the ppe^+e^- reaction are deduced and explained. The underlying models are based on Low's low energy theorem (LET), also known as soft-photon approximation (SPA).

In the first part of this chapter we will introduce the accompanying kinematics for the ppe^+e^- reaction. The dynamics of the reaction is discussed in the the second part of the chapter.

2.1 ppe^+e^- reaction observables

The cross section for the $p + p \rightarrow p + p + e^+ + e^-$ reaction is given in ref. [Kor95, Kor96] as:

$$\sigma = \frac{m_p^4 m_l^2}{(2\pi)^8 \mathrm{F}} \int |A|^2 \delta^4(p+q-p'-q'-k_+-k_-) \frac{d^3\mathbf{p}'d^3\mathbf{q}'d^3\mathbf{k}_+d^3\mathbf{k}_-}{E_{p'}E_{q'}E_{k_+}E_{k_-}}. \quad (2.1)$$

In this equation m_p and m_l are the masses of the proton and electron (positron), respectively, p, q and p', q' are the 4-momenta of the protons before and after the interaction, and k_+, k_- are the 4-momenta of the leptons. The respective 3-momenta for all particles are given in bold face, and the energy part of the 4-momentum is labelled with E. The 4-dimensional δ function enforces the 4-momentum conservation for the reaction. The flux factor is $\mathrm{F} = \sqrt{(pq)^2 - m_p^4}$, as given in [Itz80]. $|A|^2$

is the square of the transition amplitude that is discussed in the next section.

The transition amplitude contains information about the reaction dynamics. The reaction kinematics is described by the remaining part of the integral. The non-trivial integration of the final 4-body phase-space is carried out in [Kor95, Kor96] analytically in a reduced form where the solid angle of the outgoing particles was constrained. In order to compare the results of measurements with the predictions of the theoretical model, a numerical integration using a Monte Carlo method was performed. An overview of the applied method will be given in chapter 3.

2.1.1   Transition amplitude

Before we can evaluate the cross section, the matrix element of the transition amplitude has to be calculated in an appropriate coordinate system. In the analysis of the virtual bremsstrahlung the square of the transition amplitude is obtained from the coupling of the nucleonic current J_μ with the leptonic transition current j_μ. The nucleonic current leads to emission of the virtual photon $(p + p \to p + p + \gamma^*)$ while the leptonic current describes the dilepton pair $(\gamma^* \to e^+ + e^-)$ final state. The coupling is described by the transition matrix element

$$|A|^2 = \frac{e^4}{M_\gamma^4} |j^\mu J_\mu|^2, \tag{2.2}$$

where the factor $\frac{1}{M_\gamma^4}$ arises from the mass of the virtual photon in the photon propagator. To develop this expression, a summation over the lepton polarizations is performed. The square of the leptonic transition current is given in terms of a leptonic tensor

$$L^{\mu\nu} = \sum_{\text{spins}} j^\mu j^{\nu*} = \frac{1}{2m_l^2}(k^\mu k^\nu - 4l^\mu l^\nu - M_\gamma^2 g^{\mu\nu}). \tag{2.3}$$

The tensor is expressed in terms of the 4-momentum of the virtual photon $k = k_+ + k_-$ and the relative 4-momentum of the dilepton pair $l = \frac{1}{2}(k_+ - k_-)$. The metric tensor g follows the convention of [Itz80]. Using the current conservation condition $k^\mu J_\mu = 0$ the transition amplitude squared, summed over the lepton polarizations, can now be

written as

$$
\begin{aligned}
|A|^2 &= \frac{e^4}{M_\gamma^4} L^{\mu\nu} J_\mu J_\nu^* \\
&= \frac{e^4}{2m_l^2 M_\gamma^4} \left(k^\mu J_\mu k^\nu J_\nu^* - 4l^\mu J_\mu l^\nu J_\nu^* - M_\gamma^2 J^\nu J_\nu^* \right) \\
&= -\frac{e^4}{2m_l^2 M_\gamma^4} \left(4|J \cdot l|^2 + M_\gamma^2 (J \cdot J^*) \right).
\end{aligned} \tag{2.4}
$$

The nucleonic transition current J is sensitive to the nucleon-nucleon interaction and, to lesser extent, to the nucleon-photon vertex. The modelling of J will be discussed in the last section of this chapter.

2.1.2 Response functions

The cross section for the $p+p \rightarrow p+p+e^+ +e^-$ reaction can be expressed in terms of the so-called longitudinal-transverse (LT) decomposition, as usually applied for electron-scattering, [Fru84]. The LT decomposition is performed by separating the spatial part of the nucleonic current J into longitudinal and transverse components with respect to the virtual photon direction. In addition, the transverse component is further decomposed into two components corresponding to left- and right-handed circular-polarization of the virtual photon.

Following [Kor96], the LT decomposition is obtained in the coordinate system where the virtual photon direction determines the OZ axis (see Fig. 2.1). The reaction plane is given by the incoming proton direction and the virtual photon direction. Fig. 2.1 depicts the described coordinate system. As noticed in ref. [Kor95], the reaction plane is ill-defined if the photon is emitted in the (opposite) direction of the incoming proton.

The virtual photon appears as an electron-positron (dilepton) pair with 4-momenta k_+, k_-. The virtual-photon momentum is given by $k = k_+ + k_-$ and the relative virtual-photon momentum by $l = \frac{1}{2}(k_+ - k_-)$. In the coordinate system of Fig. 2.1, the vector $\mathbf{l}$ has its direction determined by the leptonic angles θ_l, ϕ_l. The polar and azimuthal angles of $\mathbf{l}$, θ_l and ϕ_l, are also called energy-sharing angle and dihedral angle, respectively.
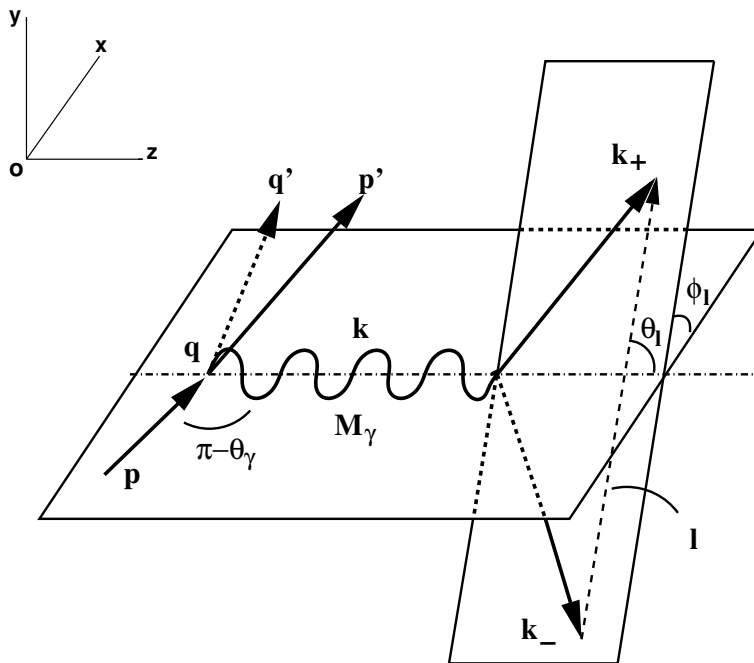
Figure 2.1: The coordinate system used in the LT-decomposition of the reaction amplitude $|A|^2$. The incoming and outgoing particles in the $p+p \rightarrow p + p + e^+ + e^-$ reaction are shown; incoming momenta of proton p, target proton q, outgoing protons p′ and q′. The outgoing virtual photon k with mass M_γ appears as a dilepton pair, i.e. electron k_- and positron k_+. The angles θ_l and ϕ_l are the polar and azimuthal angle of the relative momentum l of the dilepton pair in the given coordinate system. Note that the reaction plane is determined by the incoming proton and outgoing virtual photon, whereas the dilepton plane is spanned by the outgoing lepton momenta. Also shown is the polar angle θ_γ of the virtual photon in the lab frame.

The LT decomposition is now given by:

$$
\begin{aligned}
|A|^2 &= \frac{e^4}{2m_l^2 M_\gamma^2}\left\{ W_{\mathrm{T}}\left(1 - \frac{2\mathbf{l}^2}{M_\gamma^2}\sin^2\theta_l\right) + W_{\mathrm{L}}\left(1 - \frac{4\mathbf{l}^2}{k_0^2}\cos^2\theta_l\right)\right. \\
&\quad + \left. \frac{2\mathbf{l}^2\sin^2\theta_l}{M_\gamma^2}(W_{\mathrm{TT}}\cos 2\phi_l + W'_{\mathrm{TT}}\sin 2\phi_l)\right.
\end{aligned}
$$

$$+ \quad \frac{2l^2 \sin 2\theta_l}{k_0 M_\gamma} (W_{\mathrm{LT}} \cos \phi_l + W'_{\mathrm{LT}} \sin \phi_l) \Bigg\} . \tag{2.5}$$

The above equation is defined using the transversal W_{T}, longitudinal W_{L}, and interference $W_i, i = \mathrm{TT}, \mathrm{TT}', \mathrm{LT}, \mathrm{LT}'$ response functions (RF). The response functions W_i in Eq. (2.5) are given by:

$$
\begin{aligned}
W_{\mathrm{T}} &= J_x J_x^* + J_y J_y^* \\
W_{\mathrm{L}} &= \frac{M_\gamma^2}{k_0^2} |J_z|^2 \\
W_{\mathrm{TT}} &= J_y J_y^* - J_x J_x^* \\
W'_{\mathrm{TT}} &= -2\mathrm{Re}(J_x J_y^*) \\
W_{\mathrm{LT}} &= -2\frac{M_\gamma}{k_0}\mathrm{Re}(J_z J_x^*) \\
W'_{\mathrm{LT}} &= -2\frac{M_\gamma}{k_0}\mathrm{Re}(J_z J_y^*),
\end{aligned} \tag{2.6}
$$

where Re() takes the real part of the expression.

2.1.3 Cross section for the ppe^+e^- reaction

The cross section Eq. (2.1) can be integrated over the leptonic degrees of freedom using the LT decomposition Eq. (2.5). We start by writing Eq. (2.1) in a differential form

$$d\sigma = \frac{m_p^3 m_l^2}{(2\pi)^8 |\mathbf{p}|} |A|^2 P_{ppe^+e^-}, \tag{2.7}$$

where the flux factor $\mathrm{F} = \sqrt{(pq)^2 - m_p^4} = m_p|\mathbf{p}|$. The phase-space term $P_{ppe^+e^-}$ in this equation is

$$P_{ppe^+e^-} = \delta^4(p + q - p' - q' - k_+ - k_-)\frac{d^3\mathbf{p}'d^3\mathbf{q}'d^3\mathbf{k}_+ d^3\mathbf{k}_-}{E_{p'}E_{q'}E_{k_+}E_{k_-}}. \tag{2.8}$$

The integration over the momenta of the dilepton pair is performed by introducing the virtual photon with a 4-momentum given by $k = k_+ + k_-$, that is used to split the δ function in Eq. (2.8)

$$
\begin{aligned}
\delta^4(p + q &- p' - q' - k_+ - k_-) = \\
&= \int \delta^4(p + q - p' - q' - k)\delta^4(k - k_+ - k_-)d^4k \\
&= \int \delta^4(p + q - p' - q' - k)\delta^4(k - k_+ - k_-)d^3\mathbf{k}\,dk_0. \tag{2.9}
\end{aligned}
$$

11

Using the invariant mass $M_\gamma = \sqrt{k_0^2 - \mathbf{k}^2}$ of the virtual photon and equation Eq. (2.8), the phase-space term Eq. (2.9) can be written as

$$P_{ppe^+e^-} = P_{pp\gamma} P_{e^+e^-} M_\gamma dM_\gamma, \tag{2.10}$$

where

$$\begin{aligned}
P_{pp\gamma} &= \delta^4(p + q - p' - q' - k)\frac{d^3\mathbf{p}'d^3\mathbf{q}'d^3\mathbf{k}}{E_{p'}E_{q'}k_0} \\
&= \delta^4(p + q - p' - q' - k)\frac{\mathbf{p}'^2 d\Omega_{p'}dp'\mathbf{q}'^2 d\Omega_{q'}dq'\mathbf{k}^2 dk \sin\theta_\gamma d\theta_\gamma d\phi_\gamma}{E_{p'}E_{q'}k_0}, \quad (2.11)
\end{aligned}$$

and

$$P_{e^+e^-} = \delta^4(k - k_+ - k_-)\frac{d^3\mathbf{k}_+ d^3\mathbf{k}_-}{E_{k_+}E_{k_-}}. \tag{2.12}$$

The dilepton phase-space term $P_{e^+e^-}$ is evaluated in the rest frame of the virtual photon, ref. [Nec94], which results in

$$P_{e^+e^-} = \frac{\beta}{2}d\cos\vartheta d\varphi, \tag{2.13}$$

where $\beta = \sqrt{1 - 4\frac{m_l^2}{M_\gamma^2}}$ is the lepton velocity in the virtual photon rest frame. The angles ϑ and φ are the polar and azimuthal angle of the relative momenta of the dilepton pair in the rest frame of the virtual photon. Using the above expression we can integrate the leptonic part in Eq. (2.7). To do so, the square of the transition amplitude $|A|^2$ has to be decomposed in terms of Eq. (2.13). The longitudinal-transverse (LT) decomposition of $|A|^2$ in the lab frame given in Eq. (2.5) is Lorentz-transformed into the rest frame of the virtual photon

$$\begin{aligned}
|A|^2 &= \frac{e^4}{2m_l^2 M_\gamma^2}\left\{W_{\mathrm{T}}\left(1 - \frac{1}{2}\beta^2\sin^2\vartheta\right) + W_{\mathrm{L}}\left(1 - \beta^2\cos^2\vartheta\right)\right. \\
&+ \frac{1}{2}\beta^2\sin^2\vartheta(W_{\mathrm{TT}}\cos 2\varphi + W'_{\mathrm{TT}}\sin 2\varphi) \\
&+ \left.\frac{1}{2}\beta^2\sin 2\vartheta(W_{\mathrm{LT}}\cos\varphi + W'_{\mathrm{LT}}\sin\varphi)\right\}. \tag{2.14}
\end{aligned}$$

$|A|^2$ is further integrated over the leptonic angles ϑ and φ

$$\int |A|^2 d\cos\vartheta d\varphi = \frac{2\pi e^4}{m_l^2 M_\gamma^2}\left(1 - \frac{1}{3}\beta^2\right)(W_{\mathrm{T}} + W_{\mathrm{L}}). \tag{2.15}$$

Using $e^2 = 4\pi\alpha$, $W_{\mathrm{S}} = W_{\mathrm{T}} + W_{\mathrm{L}}$, Eq. (2.11), and the result of the above integration, the 6-fold differential cross section is obtained from Eq. (2.7)

$$\frac{d\sigma}{d\Omega_{p'} d\Omega_{q'} dM_\gamma d\theta_\gamma} = J_{\gamma^*} \frac{\alpha^2 m_p^3 \beta (1 - \frac{1}{3}\beta^2)}{16\pi^5 |\mathbf{p}| M_\gamma} W_{\mathrm{S}}. \qquad (2.16)$$

The Jacobian J_{γ^*} for $p + p \to p + p + \gamma^*$ is given by

$$J_{\gamma^*} = \int \delta^4(p + q - p' - q' - k) \frac{\mathbf{p'}^2 d|\mathbf{p'}| \mathbf{q'}^2 d|\mathbf{q'}| \mathbf{k}^2 d|\mathbf{k}| \sin\theta_\gamma d\phi_\gamma}{E_{p'} E_{q'} k_0}. \qquad (2.17)$$

An analytical expression for J_{γ^*} can be found in [Kor95].

2.2 Extraction of response functions from measured cross section

The main topic of this thesis is the analysis and interpretation of the response functions defined in Eq. (2.6). The extraction of RFs from the measured $p + p \to p + p + e^+ + e^-$ reaction is explained in chapter 3. Here we discuss the feasibility of extraction in general.

Eq. (2.5) gives us an idea how to obtain different response functions from the measured cross section. Since RFs are independent of the leptonic degrees of freedom (θ_l and ϕ_l), we can exploit the particular functional dependence on θ_l and ϕ_l of the sum in Eq. (2.5). Each of the interference RFs enters the sum as a product with orthogonal sine/cosine harmonics of the dihedral angle ϕ_l. Therefore we can weight each event with the appropriate harmonic to integrate out all other RFs and obtain the desired one. For example, to obtain W_{TT} each event has to be weighted with $\cos 2\phi_l$. For the above procedure to work well, the ϕ_l has to be covered in its full range (0-2π).

In order to probe the transversal W_{T} and the longitudinal W_{L} response functions the integration over the full range of ϕ_l is performed and the interference RFs drop out. The remaining transversal and longitudinal RFs are then separated by using the energy-sharing angle θ_l. In principle it is possible to disentangle W_{T} and W_{L} if sufficient statistics is available. In our case we constrain ourselves to two regions of θ_l chosen in such a way that in the first region $\theta_l < 40°$ the W_{T} signal is enhanced in comparison to W_{L}, and the opposite occurs in the second region. Obviously from Eq. (2.5), for the extraction of W_{T} and W_{L} we

cannot use the orthogonality property of the spherical harmonics that we use to extract the interference RFs.

In our experimental setup we were not able to distinguish between electrons and positrons. This ambiguity is reflected in the choice of the direction of the relative dilepton momenta $\mathbf{l} = \frac{1}{2}(\mathbf{k}_+ - \mathbf{k}_-)$, or rather, as a certain transformation of the leptonic angles. By interchanging two leptons the leptonic angles will be reflected in the following way

$$
\begin{aligned}
\phi_l &\rightarrow \phi_l + \pi \\
\theta_l &\rightarrow \pi - \theta_l.
\end{aligned} \tag{2.18}
$$

As it can be seen by substitution of the above expressions into Eq. (2.5), $|A|^2$ remains unaltered, thus, the choice of the lepton charge and the direction of $\mathbf{l}$ is for our purpose arbitrary. Note that this consideration holds as long as the multiplicity of the detected leptons is two.

2.3   Models

In this section we will present the theoretical models for the virtual bremsstrahlung, which are an extension of the models used to describe the real bremsstrahlung process. There are two distinctive approaches in the description of the bremsstrahlung process which are refered to as the microscopic and the macroscopic approach. The microscopic model calculation was used to compare the results of the pilot experiment [Mes99] and was developed by Martinus *et al.* [Mar98]. It is based on the OBE potential developed by Fleischer and Tjon [Fle74]. In the meantime an improved version of this potential has been published [Cos04]. For the present work, the macroscopic model calculation in the following subsection was adopted and used for comparison to the data.

2.3.1   The low-energy theorem

The macroscopic calculation used is based on the low energy theorem (LET), first proved by Low [Low58]. The theorem states that it is possible to evaluate a gauge-invariant amplitude J_μ in an expansion in the photon energy k_0 in such a way that the first two coefficients are given solely in terms of the on-the-mass-shell nucleon-nucleon phase

shifts and the on-shell NN electromagnetic vertex:

$$J_\mu = \frac{A_\mu}{k_0} + B_\mu + C_\mu k_0 + \mathcal{O}(k_0^2). \tag{2.19}$$

The approximation suggested by the theorem, in which only the first two (model independent) terms of the above expression are regarded, is also known as the soft-photon approximation (SPA). However, only the terms of order k_0 and higher are related to the off-shell properties of the NN interaction. Therefore, we have to go beyond the region of validity of the SPA to address the off-shell effects. For the case of the virtual bremsstrahlung[1] the situation is somewhat different because even for a vanishing photon momentum **k** the virtual photon mass $M_\gamma \neq 0$, which means that the intermediate nucleon is always in the off-shell state [Kor95].

By comparing the pp and pn scattering we notice that cancelation in four external legs for the pp scattering suppresses the lowest-order term in Eq. (2.19), A_μ. In the pn scattering the dominant electric dipole radiation (E1) has a strength of the order $1/k_0$, which substantially decreases the sensitivity of the bremsstrahlung process to the model dependencies. This makes the pp scattering advantageous in the study of the $pp\gamma$ reaction.

2.3.2 The virtual Low approach

In order to adapt the original Low's theorem to the virtual photon production, modifications were made in order to preserve the gauge-invariance of the reaction amplitude. The reaction amplitude for the LET calculation is expressed in terms of the on-shell NN T-matrix, which is deduced from the elastic scattering, and the static properties of the nucleon (mass, charge, and anomalous magnetic moment). Nevertheless, an ambiguity appears in the construction of the LET models, depending on the choice of the independent variables at which the on-shell T-matrix is evaluated. It was shown by [Lio93] for the case of the real photon that the ambiguity results in the introduction of two different classes of LET models.

Two different LET models have been evaluated in [Kor96] for the case of virtual photon production. The approach based on the original

---

[1]For the real photons the LET becomes model dependent only at higher energies. Contrary, for the virtual photon the LET calculation is model dependent.

Low theorem [Low58] for the real photon production and adapted for virtual photons is designated as the Virtual Low approach (VL). The other approach based on the propositions presented by Liou, Lin and Gibson in [Lio93] will be refered to as LLG approach. Both LET calculations used in this thesis are based on the T-matrix obtained from the Bonn potential [Mac96]. According to the LET the difference between two models appears in the order of k_0, the photon energy.

A general principle for the construction of the total reaction amplitude J_μ for the bremsstrahlung production is as follows; first, an external amplitude J_μ^{ext} is calculated from the leading order contributions. The total amplitude $J_\mu = J_\mu^{\text{ext}} + J_\mu^{\text{int}}$ is obtained by requiring current conservation, $k_\mu J^\mu = 0$. The internal amplitude obtained by this requirement actually represents the higher order contributions (like the meson-exchange and the rescattering diagrams that are included explicitly in a microscopic model).

From the leading-order diagrams for the real bremsstrahlung, as shown in Fig. 1.1, the external amplitude is obtained [Kor95]

$$
\begin{aligned}
J_\mu^{\text{ext}} &= T(p', q'; p - k, q)S_0(p - k)\Gamma_\mu(p - k, p) \\
&+ \Gamma_\mu(p', p' + k)S_0(p' + k)T(p' + k, q'; p, q) + (1 \leftrightarrow 2)
\end{aligned} \tag{2.20}
$$

where exchange $(1 \leftrightarrow 2)$ implies exchange between first and second nucleon: $p \to q$ and $p' \to q'$. In the above, T is the half-off-shell T-matrix and $S_0(p) = (\not{p} - m + i0)^{-1}$ is the bare nucleon propagator. Γ_μ is the reducible half-off-shell $NN\gamma$ vertex function. Here we will not go into details of the derivation of Γ_μ, which are given in [Kor95]. The right-side of the expression Eq. 2.20 is sandwiched between the nucleon spinors in the initial $u(\mathbf{p})u(\mathbf{q})$ and the final $\bar{u}(\mathbf{p}')\bar{u}(\mathbf{q}')$ state.

It turns out that condition $k_\mu J^\mu = 0$ is satisfied if J_μ^{int} obeys the relation

$$
k^\mu J_\mu^{\text{int}} = e(T(p', q'; p - k, q)\hat{e}_1 - \hat{e}_1 T(p' + k, q'; p, q) + (1 \leftrightarrow 2), \tag{2.21}
$$

where $\hat{e}_1 = (1 + \tau_z(1))/2$, τ_z being the nucleon isospin operator. To evaluate the external amplitude Eq. 2.20 the half-off-shell T-matrix is approximated by an expansion around the on-shell T-matrix $T_0 = T(p', q'; p, q)$, up to first order in k_0, or M_γ in the virtual photon rest-frame. Here we quote the final result for the total amplitude J_μ from

16

[Kor95]:

$$
\begin{aligned}
J_\mu &= e\left[\frac{p'_\mu}{kp'}\hat{e}_1 T_0 - \frac{p_\mu}{kp}T_0\hat{e}_1 + D_\mu(p')\hat{e}_1 T_0 + D_\mu(p)T_0\hat{e}_1\right.\\
&\quad -\frac{i}{2m}\left(\sigma_{\mu\nu}k^\nu\frac{\not{p}'+m}{2kp'}\hat{\kappa}_1 T_0 - T_0\hat{\kappa}_1\frac{\not{p}+m}{2kp}\sigma_{\mu\nu}k^\nu\right)\\
&\quad +\left(\frac{\gamma_\mu\not{k}}{2kp'}\hat{e}_1 T_0 + T_0\hat{e}_1\frac{\not{k}\gamma_\mu}{2kp}\right)\\
&\quad \left.-\left(\frac{p'_\mu}{(kp')^2}\hat{e}_1 T_0 + \frac{p_\mu}{(kp)^2}T_0\hat{e}_1\right)\frac{k^2}{2} + (1\leftrightarrow 2)\right],\qquad (2.22)
\end{aligned}
$$

where $\hat{\kappa} = \frac{1}{2}(1+\tau_z)\kappa_p + \frac{1}{2}(1-\tau_z)\kappa_n$, $\kappa_p = 1.79$ and $\kappa_n = -1.91$ are the anomalous magnetic moment of the proton and the neutron, respectively, and

$$
D_\mu(p) = \frac{p_\mu}{kp}k^\nu\frac{\partial}{\partial p^\nu} - \frac{\partial}{\partial p^\mu}. \qquad (2.23)
$$

The difference compared to the real photon case is in the last term of Eq. (2.22), which vanishes in the limit of the real photon $k \to 0$.

The calculation of the reaction amplitude is connected with a choice of the independent Mandelstam variables e.g. s,t or u,t at which the T-matrix is evaluated. We can define the set of Mandelstam variables used to evaluate T_0 as

$$
\begin{aligned}
s_1 &= (p+q)^2, & s_2 &= (p'+q')^2\\
t_1 &= (p-p')^2, & t_2 &= (q-q')^2\\
u_1 &= (p-q')^2, & u_2 &= (q-p')^2.
\end{aligned}
$$

In Low's original work the on-shell T-matrix is evaluated at $T_0(\bar{s},\bar{t})$ where $\bar{s} = (s_1+s_2)/2$ and $\bar{t} = (t_1+t_2)/2$. However, when the LET is applied at some finite value of k it turns out [Lio93] that $s_1 \neq s_2$, $t_1 \neq t_2$, and $u_1 \neq u_2$. For the derivation of a LET amplitude a set of independent variables t,s or t,u has to be chosen, and the point at which the T-matrix is going to be evaluated has to be defined.

2.3.3   The Liou-Lin-Gibson approach

The idea for the LLG model is based on the OBE tree-level expansion of the on-shell T-matrix. Two different approximations can be

distinguished [Lio93]: the expansion of the on-shell T-matrix into s- and t-type diagrams, and the expansion into u- and t-type of the OBE diagrams. An illustration of the two expansions is shown in Fig. 2.2. The corresponding expansions $T_0(s,t)$ and $T_0(u,t)$ lead to two different
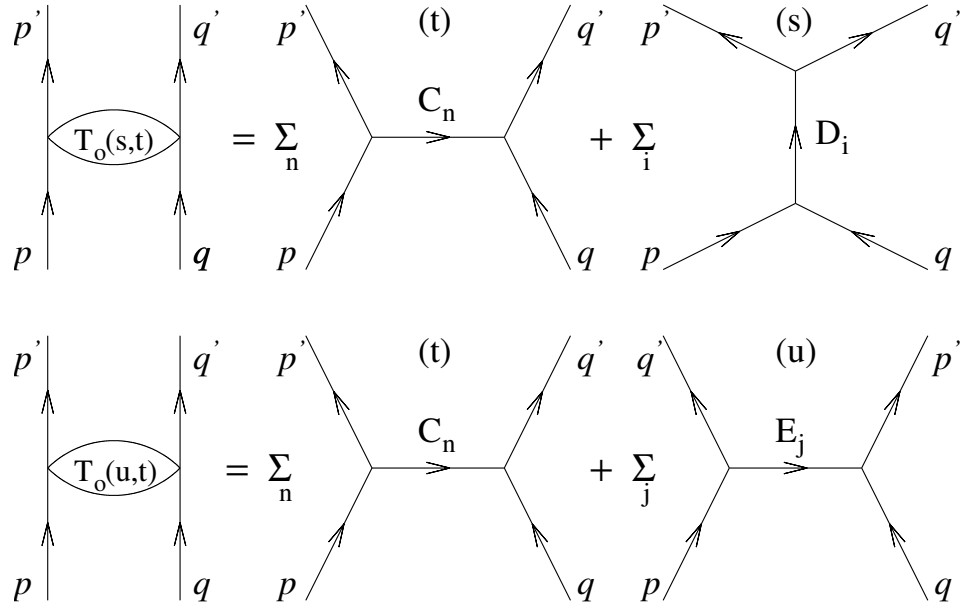

Figure 2.2: Illustration of the tree-level expansion: **top** $T_0(s,t)$ expansion and **bottom** $T_0(u,t)$ expansion. T_0 designates the pp elastic scattering T-matrix.

classes of the modified LETs. It is assumed that the $T_0(s,t)$ expansion is more suitable for the processes in which the s-channel is important, e.g. for the resonance production processes. In the meson-exchange type of process the u-channel is better suited. In the LLG model used in this work, the (u,t) expansion was applied.

The evaluation of the external amplitude for the real photon [Lio93] in the pp system is obtained by coupling the photon to each external leg of the u and t OBE diagrams. This results in an expression in which the T-matrix is evaluated at different combinations of u and t: $T_0(u_1, t_1)$, $T_0(u_1, t_2)$, $T_0(u_2, t_1)$, and $T_0(u_2, t_2)$, which is in contrast to the original Low approach in which the T-matrix is evaluated at averaged values $T_0(\bar{s}, \bar{t})$. An obvious difference to the original Low approach is

that the produced amplitude is free from the derivatives of the on-shell T-matrix, which have been replaced by finite differences.

The internal amplitude in the LLG model is obtained by coupling a photon to the intermediate boson from the OBEP. It can be expressed in terms of $T_0(u_1, t_1)$, $T_0(u_1, t_2)$, $T_0(u_2, t_1)$, and $T_0(u_2, t_2)$ [Bro83, Lio93, Kor96]. In the pp scattering where the exchange includes only the neutral mesons, this term is canceled. Similar to the original LET calculation, in order to obtain a gauge-invariant total amplitude, the gauge term J_μ^{gauge} is introduced into the total reaction amplitude $J_\mu = J_\mu^{\text{ext}} + J_\mu^{\text{int}} + J_\mu^{\text{gauge}}$. The total amplitude is calculated from the current conservation criteria.

For real photons ($k^2 = 0$) the choice of averaged Mandelstam variables results in a constant $\bar{s} + \bar{t} + \bar{u} = 4m^2 + \frac{1}{2}k^2$, contrary to virtual bremsstrahlung ($k^2 = M_\gamma^2$). In references [Kor95, Kor96] it is demonstrated that the Pauli principle for pp is violated if the averaged Mandelstam variables are used. Instead, the amplitude should be antisymmetric under the interchange of protons in the initial and the final state

$$
\begin{aligned}
\langle \bar{u}(\mathbf{p}')\bar{u}(\mathbf{q}')|j^\mu J_\mu|u(\mathbf{p})u(\mathbf{q})\rangle &= -\langle \bar{u}(\mathbf{p}')\bar{u}(\mathbf{q}')|j^\mu J_\mu|u(\mathbf{q})u(\mathbf{p})\rangle \\
&= -\langle \bar{u}(\mathbf{q}')\bar{u}(\mathbf{p}')|j^\mu J_\mu|u(\mathbf{p})u(\mathbf{q})\rangle
\end{aligned}
\tag{2.24}
$$

The violation is caused by the property of the T-matrix: $T_0(\bar{s}, \bar{t}) = -T_0(\bar{s}, \bar{t} - \frac{1}{2}k^2)$. By the original choice of averaged Mandelstam variables the symmetry would be violated in terms of order k^2. By choosing $\bar{t}$ and $\bar{u}$ as independent variables one would cure this problem but that would violate the crossing symmetry[2]. The unique choice of the Mandelstam variables which do not violate above symmetry principles turns out to be

$$
\hat{s} = \bar{s} - \frac{k^2}{6}, \ \hat{t} = \bar{t} - \frac{k^2}{6}, \ \hat{u} = \bar{u} - \frac{k^2}{6}.
\tag{2.25}
$$

From $\hat{s} + \hat{t} + \hat{u} = 4m^2$, independently of the choice of the two independent variables, both crossing symmetry and Pauli principle will be fulfilled.

2.3.4 Comparison between VL and LLG model

In Fig. 2.3 we demonstrate consequences of the LET approach by showing the difference between the two models. When the virtual photon

---

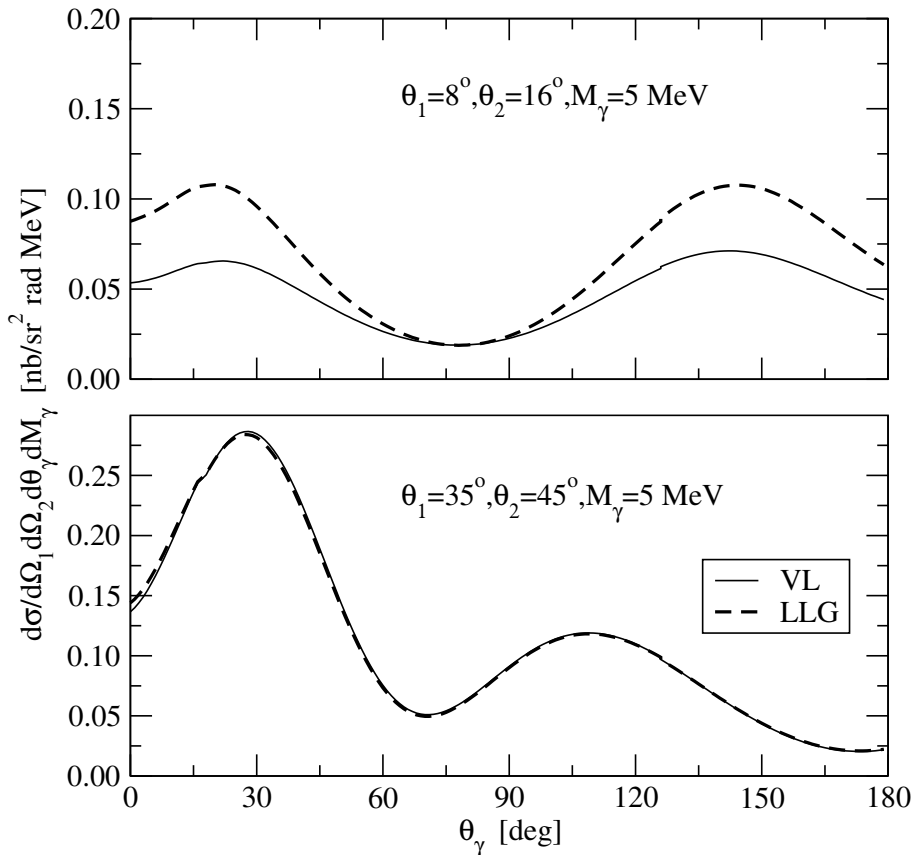[2]The crossing symmetry relates the pp and $p\bar{p}$ reactions.

Figure 2.3: The differential cross section for the $p + p \rightarrow p + p + e^{+} + e^{-}$ reaction as function of the polar angle θ_{γ} of the virtual photon. The calculation is parameterized by the lab angles of protons θ_1 and θ_2 with $\phi_1 = 0°$ and $\phi_2 = 180°$ (coplanar kinematics), and the polar angle of the virtual photon θ_{γ} and its invariant mass M_{γ}. Two different sets of parameters are chosen to illustrate the model differences. The **top** panel with $\theta_1 = 8°$ and $\theta_2 = 16°$ illustrates the situation far from elastic scattering where the virtual photon momentum k can have a large variation and therefore the model differences are substantial. The **bottom** panel demonstrates the situation where protons are close to the elastic limit ($\theta_1 = 35°$ and $\theta_2 = 45°$). The small photon momentum causes both calculations to fold to the same result.

momentum k is constrained to a small value, one can hardly observe any difference between VL and LLG model. As soon as the reaction

kinematics allows the phase-space for the larger photon momentum, a difference starts to appear. Fig. 2.4 demonstrates that this difference is more pronounced for the larger virtual photon invariant mass, i.e. larger k.
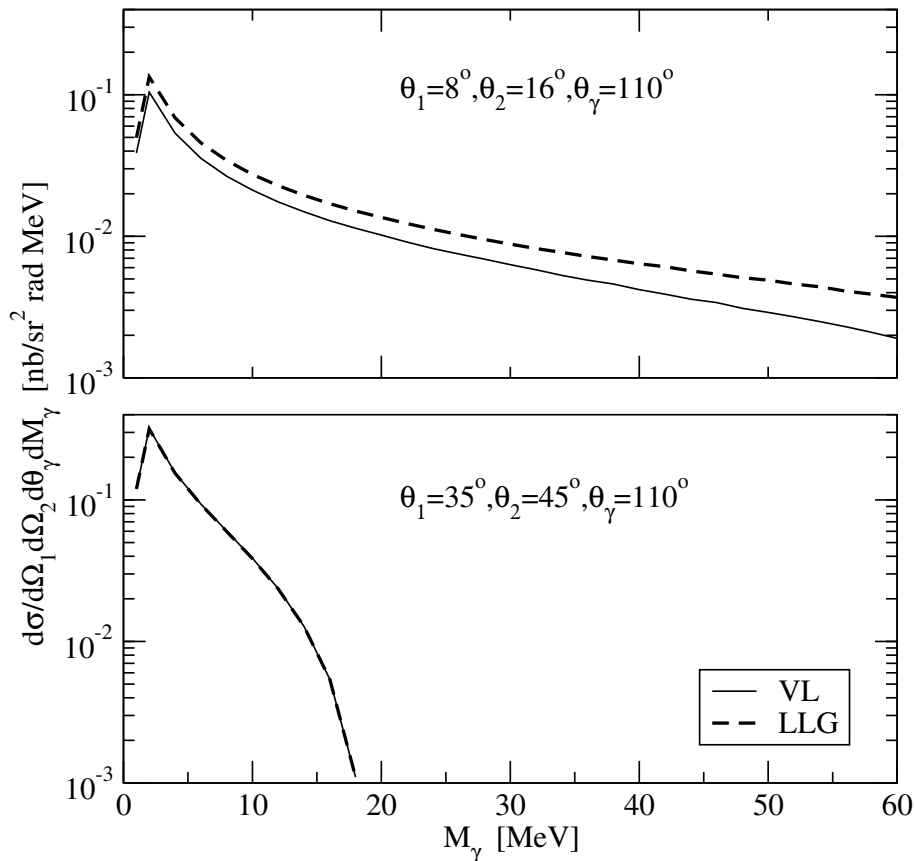

Figure 2.4: The differential cross section for the $p + p \rightarrow p + p + e^+ + e^-$ reaction as function of the invariant mass M_γ of the virtual photon. The parameters for proton angles are identical to those in Fig. 2.3 and $\theta_\gamma = 110°$. The **top** panel shows that we can observe a difference between the models, and this difference will be more pronounced at higher M_γ. In case of parameters close to the elastic limit (**bottom** panel) the difference between the models vanishes.

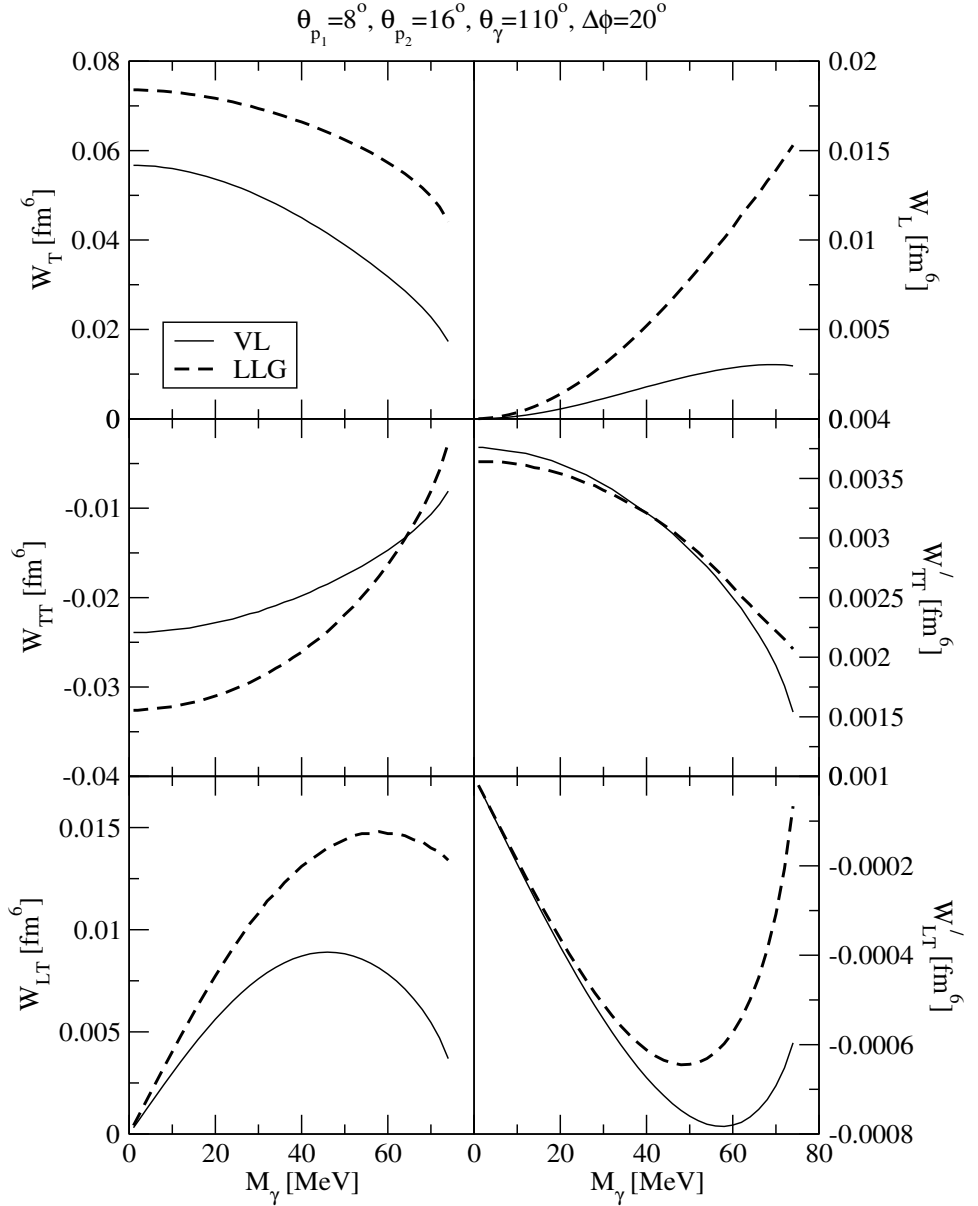The set of parameters used to obtain the response functions shown

Figure 2.5: The set of six response functions defined by Eq. 2.5, calculated for both the VL and LLG models, and presented as functions of the invariant mass M_γ.

in Fig. 2.5 is similar to the one used to obtain the cross section shown in Fig. 2.4, apart from the fact that the non-coplanarity angle $\Delta\phi = \pi - (\phi_{p_2} - \phi_{p_1})$ was set to $\Delta\phi = 20°$. In both Figs. 2.3 and 2.4 we have used the calculations for the coplanar kinematics, $\Delta\phi = 0°$. Due to the symmetry properties of the response functions [Kor96] both W'_{TT} and W'_{LT} vanish in case of the coplanar kinematics. The difference between the two models for different RFs is clearly observed. The most striking difference is shown in the calculation of W_{L} where the LLG model predicts a large contribution at the higher invariant masses M_γ. Note that the LLG model gives an overall larger estimate of the cross sections as well.